Correlation of elastic and mechanical properties of consolidated granular media during microstructure evolution induced by damage and repair

A. S. Gliozzi,[1] M. Scalerandi,[1] G. Anglani,[2] P. Antonaci,[2] and L. Salini[1,2]
[1]*Department of Applied Science and Technology, Condensed Matter and Complex Systems Physics Institute, Politecnico di Torino, Italy*
[2]*Department of Structural, Geotechnical and Building Engineering, Politecnico di Torino, Italy*

(Received 27 June 2017; revised manuscript received 2 November 2017; published 5 January 2018)

Evolving cracks in consolidated granular media cause a modification of the microstructure in the area surrounding the damaged zone. As a consequence, the mechanical properties (flexural strength) and the elastic characteristics (linear modulus and nonlinear parameters) change as well. The same happens during repair, which could be considered as the symmetric counterpart of mechanical damaging. Starting from ultrasonic measurements of the resonance and nonlinear properties of concrete prisms during progression of damage and repair, we propose a description of the microstructure evolution, which allows to predict the observed phenomenology. Also, we demonstrate the existence of a correlation between ultrasonic elastic parameters and mechanical properties of the samples at each damage/repair state, pointing out symmetries and differences observed in the two processes.

DOI: 10.1103/PhysRevMaterials.2.013601

I. INTRODUCTION

Cracks propagation in consolidated granular media corresponds to an evolution of their microstructure, for instance, through the generation of clapping [1] or Hertzian contacts [2] in the crack area or through the nucleation of dislocations [3] in a small area surrounding the crack zone. Repairing could be seen as the symmetric counterpart of mechanical damaging since, either in autonomic systems [4–6] or in external repair methods [7,8], the activation of a repairing agent in the damaged area causes a regression of the crack extent. The analogy of damaging and healing processes in consolidated media with the rearrangement, aging, and relaxation effect in nonconsolidated granular media [9–11] is quite evident.

Usually, repairing agents have different mechanical and elastic properties with respect to those of the original consolidated granular medium, but in some cases they may react with it at the crack interface in such a way to make the interaction zone substantially equivalent to the original material after a given healing time. This is the case, for example, of alkaline silicates reacting with a hardened cement matrix [12,13].

Even though the material microstructure is affected only in a small area surrounding the crack zone, effects on the overall mechanical performances can be significant [14,15]. In particular, the ultimate flexural strength (corresponding to the maximum load that can be carried in a given configuration) is very sensitive to the contact area, thus to the presence of local damage [16].

The presence of imperfections or contacts at the crack surfaces or in the surrounding zone also influences the elastic properties of the medium. On one side, the medium behaves with effective elastic modulus and damping which differ from the corresponding properties of the intact material. Such a linear effect could be easily detected and quantified by considering the resonance spectrum of the sample in a given frequency bandwidth [17,18]. On the other side, the nonlinear elastic parameters of the medium are even more sensitive to small variations of the local microstructure [19,20]. They can be quantified by analyzing the resonance frequency [21,22], the higher-order harmonics [23,24], the break of the superposition principle [25–28], the wave-mixing effects [29], the subharmonics generation [30], and others.

Experimental evidences indicate that increasing the cracks density or the cracks extension in consolidated granular media causes a reduction of the ultimate flexural strength [16], softening phenomena [17], and increase of the nonlinear elastic parameters [31,32]. During the inverse mechanism, increasing the duration of the curing process after the application of a repairing agent on a damaged interface (i.e., increasing the so-called "healing time"), causes a regain of mechanical strength [33–36] and a recovery of elastic linear and nonlinear properties [12].

Although experimental observations show similarities between the evolution of the mechanical and elastic parameters during damage and repair progression, the link between their variations and the microstructure evolution is yet to be fully explored. The goal of this contribution is to demonstrate the existence of a correlation between mechanical strength and elastic parameters (linear modulus and nonlinear properties). Considering the similarities and differences in their evolution during damaging and repairing, we also aim to propose a description of the microstructural evolution, as suggested by the ultrasonic analysis of the variations of the elastic properties.

To achieve these goals, experiments and simulations were performed. The experiment setup and configuration are discussed in Sec. II. Starting from intact samples, first progressive damage was induced by means of three-point bending tests [37], conducted in displacement control up to failure. During this stage, ultrasonic indicators of the linear [18] and nonlinear [25] elastic properties were measured and analyzed as a function of damage progression. In a subsequent stage, the residual fragments resulting from the three-point-bending test were reassembled using a sodium silicate solution as a repairing agent [12,13,38]. Then, the same ultrasonic indicators of linear and nonlinear elastic properties were measured and analyzed

as a function of time since the repairing action provided by the sodium silicate solution is not immediate, but is expected to evolve during the healing time. The experimental results are discussed in Sec. III. A second set of samples, subjected to the same damaging and repairing procedure, was mechanically tested at different ages in the course of the repair process, to obtain the temporal evolution of their mechanical strength as a function of healing time. The results of the mechanical and ultrasonic tests were correlated in the first part of Sec. IV. To link the experimental observations with the evolution of the microstructure in the area affected by damage progression, numerical simulations based on a multistate Preisach-Mayergoyz description [39–46] were performed and the corresponding results are reported in the second part of Sec. IV.

II. EXPERIMENTAL ANALYSIS

A. Materials

The specimens used for this study were in the shape of ($4 \times 4 \times 16$ cm^3) concrete prisms with a U-shaped notch 4 mm long and 4 mm wide at mid-span. The concrete matrix was produced using a CEM I 52.5 R cement, a water-to-cement ratio of 0.5 and a cement-to-sand ratio of 1:3 by weight, in accordance with [37]. After casting, the samples were stored in their molds for 24 h, subsequently in water for 28 days, then in a low-temperature drying oven for additional 24 h, and finally in the laboratory for testing.

Starting from samples in their "intact state," a pass-through crack was generated at mid-span by a sequence of three-point-bending test cycles with controlled displacement rate at the edge of the notch. Each test cycle was conducted in such a way to achieve a progressively increasing stress and strain state, so as to induce crack initiation at the notch, crack propagation through the specimen cross section, and finally creation of a complete disconnection between the two halves of each prism. In the following, the relative displacement of the edges of the notch, that corresponds either to an elastic elongation (in the initial loading cycles prior to crack propagation) or to an actual crack mouth opening displacement (during the crack propagation cycles), will be simply referred to as "displacement" (v) for the sake of brevity. The loading sequence was interrupted at preselected values of displacement in order to ultrasonically test the samples in different states.

At the end of the damage process, i.e., when the sample was broken into two halves, a thin layer of sodium silicate solution was applied manually to the crack surface, with the aim to reassemble the two residual fragments, thanks to the activation of the healing process, which would induce the progressive creation of a stable bond between the opposite edges of the fractured zone, bridging them together, and eventually restoring the material integrity. Alkaline silicates are widely used for concrete consolidation purposes because of their low viscosity, which enables them to effectively diffuse through the cracks, and also owing to their chemical affinity with the cement matrix [12,13,38]. The residual crack width after reassembling was evaluated by means of a 20× optical microscope, resulting in around 500 μm, on average. In continuity with previous studies [5,12], the sodium silicate used was provided by Sigma Aldrich and was characterized by a 10.6 wt.% proportion of Na_2O, a 26.5 wt.% proportion of SiO_2, and a 62.9 wt.% of water.

Some repaired specimens were monitored ultrasonically for a long time during the repair phase, while some others were subjected to three-point-bending tests at different ages during the repair process (i.e., at different "healing times") to determine their mechanical properties. Such mechanical tests being destructive, they could not be performed at different times during the healing process on the same samples as the ones subjected to the ultrasonic measurements, but they had to be carried out on other samples, identical to the ones ultrasonically monitored.

B. Mechanical testing

As anticipated in the previous section, flexural tests were performed to induce a controlled damage process, and subsequently to evaluate the recovery of mechanical performance as a function of healing. This is a well-established practice in the field of self-healing concrete assessment since it allows to produce cracks in an easier and more controllable way than tensile tests, plus it makes it possible to express the mechanical performance recovery very effectively, as regain of load-carrying capacity [33,34]. Different mechanical quantities, such as stress intensity factor or toughness, could also be used to characterize the material recovery.

All the tests were carried out with the aid of a 250-kN servocontrolled hydraulic testing machine working in displacement control. A test rate of 1.5 μ/s was imposed by means of an HBM DD1 displacement transducer mounted in correspondence of the edges of the notch.

For each cycle of the loading sequence described in the preceding subsection, load versus displacement curves were recorded, as reported in Fig. 1 as an example. Here, Figs. 1(a)–1(c) display a few selected curves for one of the prisms tested (black lines), while Fig. 1(d) shows the superposition of the curves corresponding to the entire loading sequence [their envelope is also reported in Figs. 1(a)–1(c) as a dashed blue line]. In Fig. 1(e), load vs displacement curves are shown for different prisms tested after repair, at different healing times.

Each cycle was performed starting from a different mechanical state: "undamaged" for loading cycles performed up to reaching the maximum load in the envelope curve [e.g., Fig. 1(a)], "damaged" for the following loading cycles [e.g., Figs. 1(b) and 1(c)] or "partially healed" for the cycles performed during healing [e.g., Fig. 1(e)]. For the undamaged states, the maximum flexural solicitation that the sample can bear is given by the peak load of the envelope curve [y coordinate of the blue diamond in Figs. 1(a) and 1(d)]. It is related to the flexural strength of the material (also referred to as "ultimate flexural strength") and will be denoted by L_u. The x coordinate of the blue diamond peak represents the maximum elastic elongation v_u that the specimen can bear before initiation of crack propagation. For the damaged states, the flexural strength is normally termed "residual strength" since it decreases with increasing damage; therefore, at the beginning of each cycle in the damaged states, the residual flexural strength is just a fraction of the ultimate strength [see green diamonds in Figs. 1(b)–1(d), with load values denoted by L_r]. For the partially healed states, the flexural strength of the sample

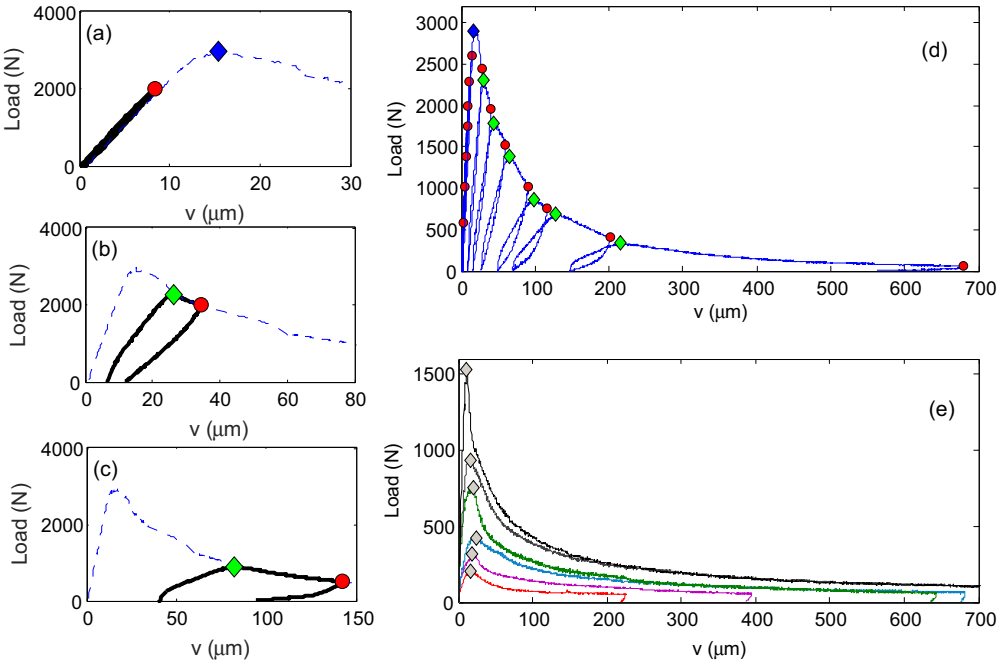

FIG. 1. Load versus displacement curves from three-point-bending tests: (a)–(c) A few selected cycles performed during the entire loading sequence. Once the stress-strain state corresponding to red circles was reached, the sample was unloaded and subjected to ultrasonic tests. (d) Superposition of all tests performed during the loading sequence. Again, red circles denote the points at which the test was interrupted to allow for ultrasonic measurements. (e) Tests performed on prisms at different healing times. In all curves, the y coordinate of the diamond points corresponds to the actual flexural strength for the given state of the sample.

increases significantly with increasing healing time [see gray diamonds in Fig. 1(e), with load values denoted by L_h].

Throughout the loading sequence, cycles were interrupted after reaching a prefixed displacement, termed v_s, corresponding to the x coordinate of the red circles in Figs. 1(a)–1(d) and ultrasonic testing was performed. To quantify the state of the sample at each cycle, a damage parameter D was introduced:

$$D = 20 \log_{10}(v_s/v_u). \tag{1}$$

The condition $D > 0$ means that the maximum elastic elongation is overcome, so that a flexural crack is initiated and starts to propagate. Hence, the definition of "damaged" state. Conversely, as long as $D < 0$, the sample is "undamaged" given that the maximum elastic elongation is not overcome yet.

C. Ultrasonic testing

1. Experimental setup

Each sample was ultrasonically tested both during the damaging and the repairing phases. To allow measurements, each sample was equipped with two identical narrow-band piezoelectric transducers glued with a linear coupling agent (phenyl salicylate) to the bases of the prism, acting as an emitter and a receiver, respectively. Transducers had a diameter of 4 cm, a central frequency at 55.5 kHz, and an almost flat response between 10 and 40 kHz. Transducers were glued to the intact samples and never removed up to the end of the monitoring.

The emitting transducer was connected to an arbitrary waveform generator (Agilent 33500B) through a 20× linear amplifier (FLC Electronics A400). A rectangular pulse signal with width $\Delta t = 10\ \mu$s was chosen as an input. Excitation amplitude ranged from 200 mV (i.e., the lowest amplitude allowing detection of a signal emerging from noise) to 12 V (much lower than the highest amplitude at which the experimental setup was known to behave linearly). The receiving transducer was connected to an oscilloscope (Agilent Infinium DSO9024H) for data acquisition. Resolution was set to 13 bits and sampling rate to 10 MSa/s. Signals were recorded in a 10-ms time window. Averaging was used (over 64 signals) to improve the signal-to-noise ratio. The linearity of the experimental setup was carefully tested in the range of amplitudes adopted.

For each sample (on a total of six), the evolution of the ultrasonic parameters was monitored. First, measurements were taken at increasing damage levels [as quantified by the parameter D, see Eq. (1)]; then, in the following four weeks, measurements were taken at successive times to monitor the repair process. In each acquisition we recorded for each sample a set of nine signals $u_i(t)$ at increasing amplitude of excitation in the range $0.2\ \text{V} < A_i < 12\ \text{V}$.

It is worth pointing out here that the samples were assumed to be substantially homogeneous, due to the production and curing procedures adopted: indeed, as previously described, all the specimens were manufactured simultaneously, starting from the same fresh concrete mix (hence with the same sand, cement, and water proportions) and they were cured and stored in the same environmental conditions. Plus, the use of a standardized sand in accordance with Ref. [37] guaranteed a proper granulometric assortment, with consequent maximum packing and uniform distribution of the solid grains. Minor inhomogeneities might, however, be present, though they are not expected to affect the ultrasonic experiments from a

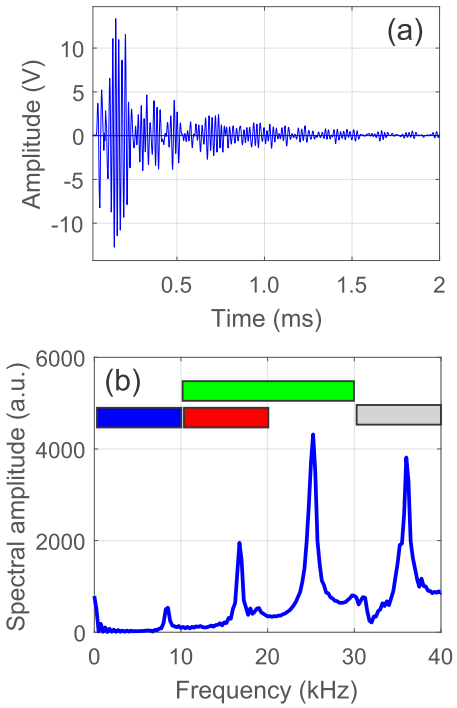

FIG. 2. (a) Temporal signal detected on one of the intact samples. (b) Spectrum of the temporal signal reported in (a). Rectangular colored bands in the plot indicate the frequency bandwidths used for the definition of the ultrasonic indicators discussed in the text.

practical point of view due to their negligible size as compared to the wavelength here used.

In addition to the composition-related factors mentioned above, some other sources of variability might be present, due to small differences in the positioning of the notch and in the coupling of the transducers: they can result in small variations of the measured ultrasonic quantities among the different specimens, as it will be detailed in the following.

2. *Linear measurements*

A portion of the temporal signal recorded on an intact sample at a given amplitude of excitation is shown in Fig. 2(a). The signals detected during the damaging and the repairing phases have a similar aspect. However, with increasing damage, we notice a progressive distortion, as well as a reduction in amplitude due to increase of attenuation. During the repairing phase, with increasing time, we notice an almost full recovery of the original signal shape.

The distortions of the signals can be properly described through a spectral analysis. To do so, the spectra of the detected signals were calculated by means of a fast Fourier transform (FFT) algorithm implemented through the MATLAB FFT function (with rectangular windowing and 10^5 points, corresponding to the entire duration of the signal). An example is shown in Fig. 2(b). Typically, the spectra present four main peaks (at approximately multiple frequencies) which correspond to the four longitudinal resonance modes of the sample. Other peaks may be present, corresponding to other modes, but they are not relevant in this context. For the sample considered in Fig. 2, the first four resonance frequencies correspond to

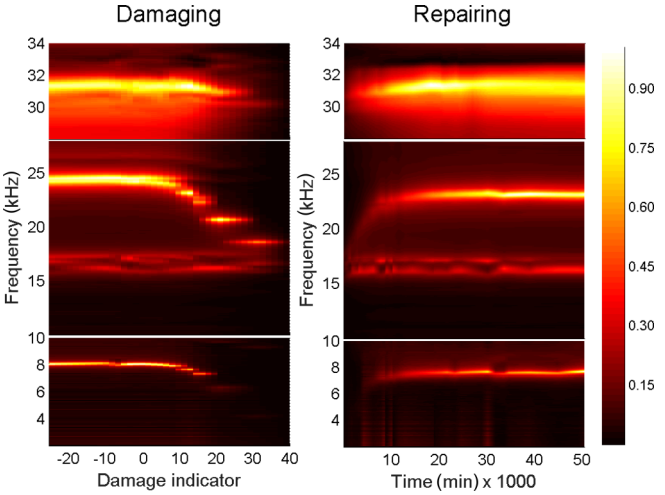

FIG. 3. Spectral response of signals detected on one sample during the damaging (left column) and repairing (right column) phases, plotted vs the damage indicator D [see Eq. (1)] and healing time, respectively.

$\omega_r \approx 9$, 18, 27, and 36 kHz, although they are not exactly multiple, due to dispersion effects and/or geometrical features. As we will show in Fig. 3, the resonance modes differ slightly from one sample to another, though such differences are minor. On the whole, four frequency bandwidths could be identified, each one including one resonance mode, as shown with rectangular color bands in Fig. 2(b).

As mentioned, distortions of the signals in the damaged and intermediate repairing stages correspond to an evolution of the spectrum, which is discussed in Fig. 3. Here, we consider a different sample with respect to the one used in Fig. 2, to bring the reader's attention to the possible variations occurring in the measured ultrasonic quantities due to stochastic differences in the positioning of the notch and in the coupling of the transducers, further than to other minor composition-related factors. In Fig. 3, we show the spectral amplitudes as calculated based on the raw signals recorded from the piezoelectric transducers at each damage level (left column) and each healing time (right column) using a color map representation. For this sample, the first longitudinal mode is slightly lower (around 8 kHz) than for the sample tested in Fig. 2. The color scale is normalized to one in each of the three bandwidths considered, i.e., corresponding to those marked with blue, green, and gray rectangles in Fig. 2(b). Due to different normalizations in the three frequency bands, amplitudes of the modes should not be compared.

The evolution of the spectra could be discussed as follows:

(i) Damaging phase (left column): with progressively increasing damage, even resonance frequencies survive (16 and 32 kHz), progressively diminishing in amplitude; odd resonance frequencies slowly shift to lower values up to disappearing due to high increase of attenuation. In particular, the third mode coalesces with the second mode. It is interesting to note that the spectral evolution is negligible up to $D = 0$, which means that almost no changes in the sample microstructure are introduced up to reaching the conditions for crack propagation in three-point bending.

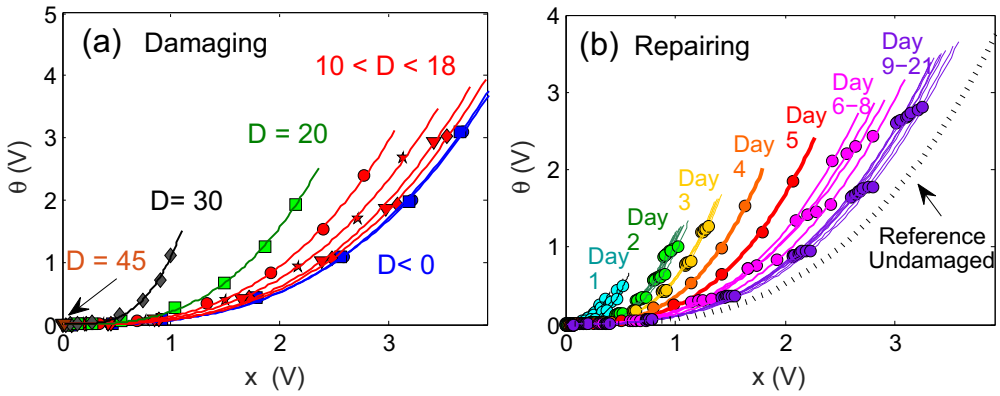

FIG. 4. Nonlinear measurements on one of the tested samples. The SSM indicator θ is shown versus the maximum amplitude of the output signals x during the damaging and repairing phases. A power-law relationship between the two quantities is found in accordance with Eq. (3). Fitting of the data indicates that the exponent b is roughly constant for all curves and samples. Thus, here and in the following, fits were performed by varying only the coefficient a and assuming $b = 2.5$.

(ii) Repairing phase (right column): the evolution of the spectrum as a function of healing time is symmetric. With increasing time, odd resonances reappear (the third mode splitting out of the second mode) and the spectral amplitude (at all frequencies) increases significantly. Almost full recovery is obtained.

The behavior shown here was detected on one of the analyzed samples, but a similar behavior was observed on the entire set of six samples. A more quantitative discussion will be provided in the next section.

3. Nonlinear measurements

As discussed above, in each state of the sample, measurements were performed by increasing the amplitude of excitation in order to highlight the presence of nonlinear effects. In the analysis reported here, the nonlinearity of the sample is analyzed using the scaling subtraction method (SSM) [25–27], in which the amplitude dependence of the elastic properties is estimated using the break of proportionality principle.

The method is very simple and its implementation consists in the following steps:

(i) The sample is excited with a pulse at the lowest amplitude A_0 in such a way that the propagation could be assumed as almost linear (in our case, $A_0 = 200$ mV). The corresponding output signal $u_0(t)$ is recorded and windowed in a given time window starting with the first arrivals (we used a signal window $\Delta t = 0.1$ ms);

(ii) The sample is excited with the same source function but at a higher amplitude A_i. Again, the corresponding signal $u_i(t)$ is detected and recorded. Synchronization with the previous excitations is ensured;

(iii) If the system was linear, it is expected that $u_i(t)/A_i \approx u_0(t)/A_0$, with small discrepancies due to noise effects [47]. Therefore, the contribution due to nonlinearity at amplitude A_i is fully contained in the SSM signal $w_i(t)$:

$$w_i(t) = u_i(t) - A_i u_0(t)/A_0. \tag{2}$$

(iv) The nonlinear contribution at the excitation amplitude A_i is here defined as $\theta_i = \max[w_i(t)]$. It can be plotted as a function of the maximum strain amplitude of the propagating ultrasonic wave, assumed to be proportional to the maximum amplitude x_i of the signals $u_i(t)$ in the same time window.

In Fig. 4, we report some θ versus x curves recorded during damage and repair. The symmetry between the two processes is remarkable. In the damaging phase [Fig. 4(a)], nonlinearity is substantially constant up to reaching the material ultimate strength ($D \leqslant 0$). As soon as the crack is initiated and starts to propagate, nonlinearity begins to increase.

During the repairing phase [Fig. 4(b)], nonlinearity diminishes rapidly in the first seven days. The original intact state (corresponding data are reported for reference as a dashed line) is not completely recovered. In both plots, the solid lines refer to a power-law fitting of the data in the form

$$\theta = a(x/x_0)^b, \tag{3}$$

where $x_0 = 1$ V is introduced to make the power-law exponent b adimensional.

III. EVOLUTION OF LINEAR AND NONLINEAR PARAMETERS

In this section, three ultrasonic indicators will be defined in order to allow for a quantitative analysis of the data presented in the previous subsection.

A. Linear spectral analysis

The spectrum reported in Fig. 2(b) highlights the presence of odd and even resonance peaks in the response of the intact samples. Odd resonances shift during both damaging and repairing phases. In principle, we can define four frequency bandwidths of a few kHz centered around each resonance peak to include the single resonance frequency values and the related variations due to shifting [colored rectangles in Fig. 2(b)]. One exception is introduced to monitor the evolution of the third resonance mode, for which the frequency bandwidth should be larger than the others [green rectangle in Fig. 2(b)], because it showed a greater shift during damaging and repairing phases. Therefore, to quantitatively characterize the spectrum,

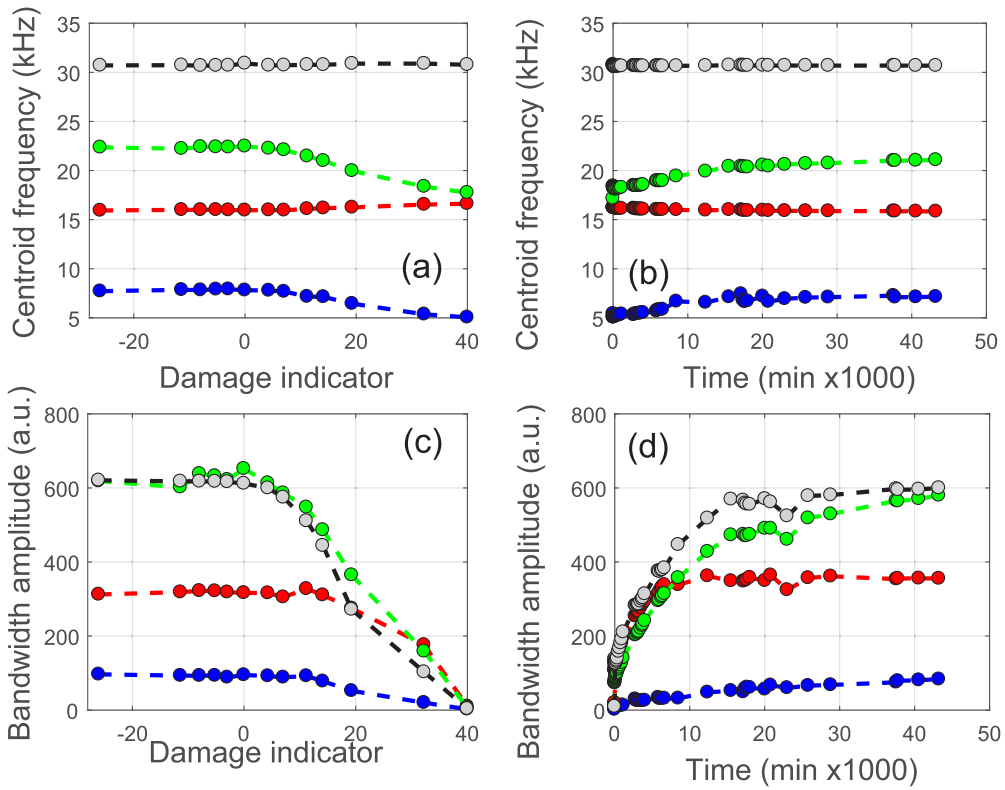

FIG. 5. Centroid frequency and bandwidth amplitude during the damaging (left column)and repairing (right column) phases. Different colors refer to the indicators defined in the four frequency bands specified in the text and shown as rectangles in Fig. 2(b).

we divided it into four regions. For most of the samples, a frequency bandwidth of 9 kHz was chosen:

(a) 0 kHz $\leqslant \omega <$ 9 kHz: containing the first resonance mode;

(b) 9 kHz $\leqslant \omega <$ 18 kHz: containing the second resonance mode;

(c) 9 kHz $\leqslant \omega <$ 27 kHz: containing the second resonance mode and the third resonance mode (the last one being dominating in amplitude);

(d) 27 kHz $\leqslant \omega \leqslant$ 36 kHz: containing the fourth resonance mode.

In the case of a few samples, a larger interval of 10 kHz was chosen (as for the case of Fig. 2) due to the different modes distribution.

In each region, we characterize the spectrum introducing two quantities which quantify the "position" of the peak (centroid frequency) and the "amplitude" of the peak (bandwidth amplitude). The two quantities are defined as follows:

$$\omega_c = \frac{\int_{\omega_L}^{\omega_H} A_\omega \omega \, d\omega}{\int_{\omega_L}^{\omega_H} A_\omega d\omega}, \tag{4}$$

$$\Lambda_c = \int_{\omega_L}^{\omega_H} A_\omega d\omega. \tag{5}$$

Here, ω_L and ω_H indicate the lower and upper frequency limits of each of the four frequency bands described above. Since the calculations are performed for each frequency band, four couples of indicators will be available.

It is interesting to observe that the above-defined quantities ω_c and Λ_c are closely related to the elastic modulus of the material and to the acoustic quality factor, respectively. Recent papers [48] have pointed out how their variations are strictly dependent on the variation of the concentration of the defects, with direct analogy with the approach followed in this study. We also remark that the quantities discussed have analogies with the resonance frequencies and Q factor measured in nonlinear resonance ultrasound spectroscopy experiments, where, albeit in a different context, it was found that the damping contribution is normally more sensitive to the presence of defects than the resonance frequency shift [21,49,50]. Our results confirm this observation.

The centroid frequencies and bandwidth amplitudes are shown in Fig. 5 for one of the tested samples as a function of damage progression and healing time (as during damaging and repairing phases, respectively). The decrease (increase) in frequency of the odd peaks during damaging (healing) is evident and regular. Likewise, the plot well captures the decrease/increase in the amplitude of the four peaks. It is also important to observe the time scales on which the evolution takes place. During the damaging phase, we do not appreciate any effect up to reaching the material's ultimate strength ($D = 0$). During the repairing phase, all curves reach an asymptotic value within approximately 28 days (corresponding to 4×10^4 min). We also point out that a slightly different time scale can be observed for the second resonance (red curve), where amplitude stabilization is reached in about 7 days (corresponding approximately to 10^4 min), while no peak shift is manifested.

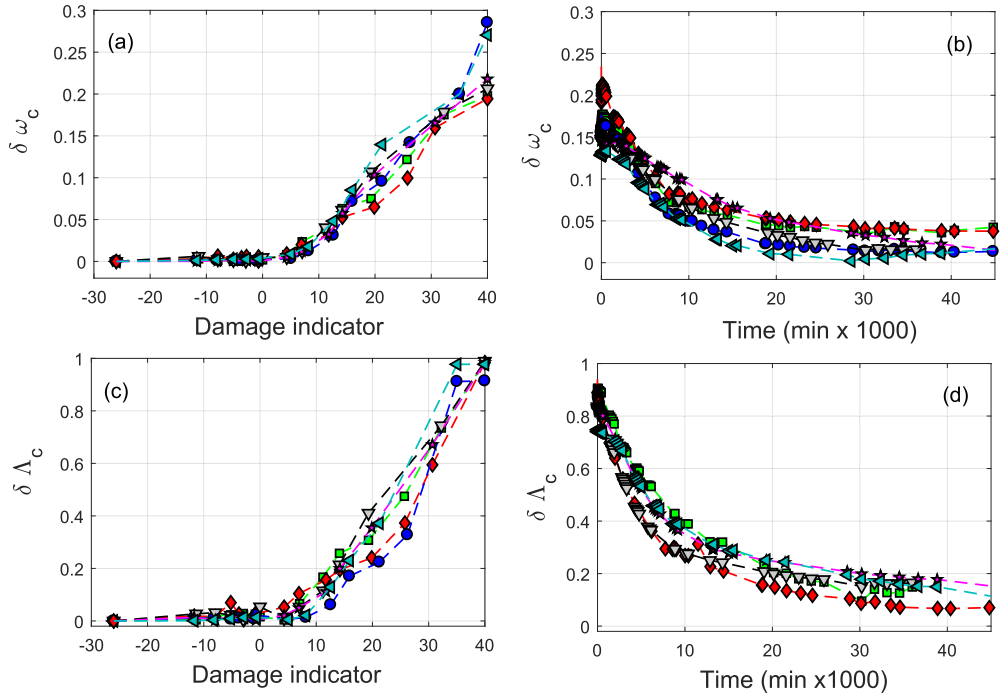

FIG. 6. Relative variation of the centroid frequency and bandwidth amplitude with respect to the values assumed for the intact sample, calculated for the third resonance mode [green bandwidth in Fig. 2(b)]. Curves obtained on the six samples analyzed are well overlapped. (a) Evolution during the damaging phase; (b) evolution during the repairing phase.

The qualitative behavior observed for the overall set of specimens was always the same, as shown in Fig. 6. Here, the variations of the two indicators with respect to the values assumed for the intact sample are shown (with reference to the bandwidth containing the third resonance mode), according to Eq. (6):

$$\delta\omega_c = \frac{\omega_c - \omega_c^{\text{intact}}}{\omega_c^{\text{intact}}},$$
$$\delta\Lambda_c = \frac{\Lambda_c - \Lambda_c^{\text{intact}}}{\Lambda_c^{\text{intact}}}. \quad (6)$$

A similar level of repeatability can be also noticed for the indicators calculated in the other three frequency bandwidths. After repairing, the variations of both indicators almost turn back to zero.

B. Scaling subtraction method

A quantitative indicator could be defined also for the nonlinear ultrasonic parameters. The nonlinear indicator θ depends on the maximum output amplitude x according to a power-law behavior [see Eq. (3)]. Since the exponent b is substantially constant during all phases of damaging and repairing ($b \approx 2.5$), the coefficient a fully defines the nonlinear behavior.

The nonlinear indicator used to monitor the evolution of nonlinearity during the damaging and repairing phases is defined as the variation of the coefficient a with respect to the value a^{intact} which was measured when the sample was intact:

$$\delta a = \frac{a - a^{\text{intact}}}{a^{\text{intact}}}. \quad (7)$$

In Fig. 7, δa is plotted during the damaging and repairing phases for three samples with different colors. The parameter increases with increasing damage. Again, after repairing the variation of the parameter is almost turned back to zero, denoting excellent, but not complete, recovery. We also notice that the time scale for recovery of the nonlinear parameters appears to be different than the time scale for recovery of the linear parameters (centroid frequency and bandwidth amplitude). In fact, full recovery is obtained after approximately 7 days (corresponding to 10^4 min). The repeatability of the nonlinear measurements is also excellent.

IV. DISCUSSION

A. Link with mechanical parameters

As shown in the previous section, the ultrasonic linear and nonlinear parameters evolve with increasing damage and healing time with a symmetric behavior. The mechanical characteristics of the examined samples, and in particular their load-carrying capacity related to the actual flexural strength, vary as well as a function of damage progression [Figs. 1(a)–1(d)] and healing time [Fig. 1(e)].

In order to establish a correlation, in Fig. 8 the ultrasonic parameters measured on different samples are shown as a function of the load-carrying capacity corresponding to their actual flexural strength. When considering the entire loading

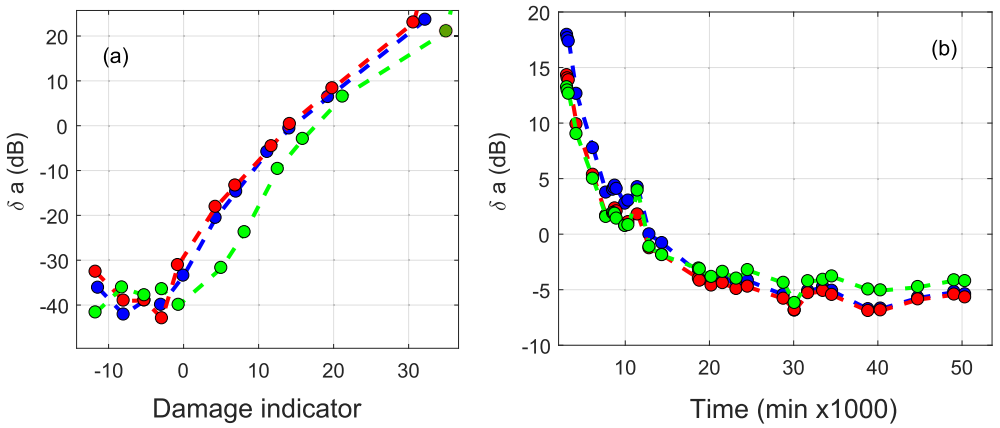

FIG. 7. Nonlinear ultrasonic parameter δa (relative variation of a with respect to the value it assumed when the sample was intact) during damaging and repairing phases. Different colors refer to measurements obtained on different samples.

sequence, the actual flexural strength is the ultimate strength (hence L_u) for $D < 0$ or the residual strength (then L_r) for $D > 0$, while in the repairing phases the actual flexural strength is derived from the average of peak values L_h resulting from the mechanical tests performed on sets of five additional repaired samples at the same healing time as the ultrasonic measurements. In the case of the linear ultrasonic parameters, we presented only the bandwidth amplitude indicator calculated for the third resonance mode, but similar results were obtained for the centroid frequency indicator too and for the first resonance mode.

As already remarked, as far as the loading sequence is concerned, ultrasonic tests and mechanical tests could be performed on the same specimens (six, on the whole), thus, we have a one-to-one correspondence between ultrasonic indicators and mechanical parameters. This feature could not be preserved in the repairing process due to the destructiveness of the mechanical tests conducted to determine the flexural strength. Therefore, in the repairing phases, the first set of six samples was monitored ultrasonically for a total time of more than 4 weeks and the ultrasonic indicators for each healing time were obtained by averaging the measurements

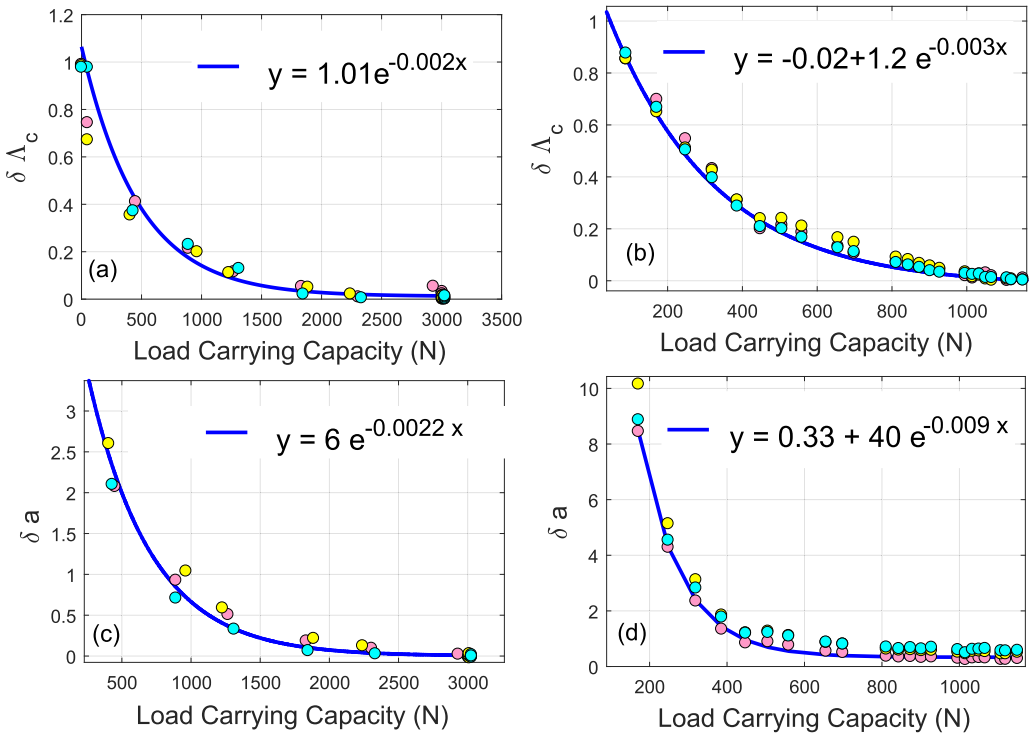

FIG. 8. Correlation between linear and nonlinear ultrasonic parameters and mechanical parameters. Measurements of the linear indicator are performed in the frequency bandwidth of the third resonance mode. Results are shown for a selection of samples during the loading sequence [(a) and (c)] and healing time [(b) and (d)]. The load-carrying capacity, depending on the actual flexural strength, is calculated as a function of the L_u, L_r, and L_h values recorded during the mechanical tests.

performed on the same sample at the given healing time (i.e., all the measurements taken within the same day); in parallel, mechanical tests were performed on other sets of specimens, each one composed of five samples and tested at the same healing time as in the ultrasonic monitoring, thus allowing to calculate the average flexural strength of the repaired samples. The good repeatability of the measurements discussed in the previous section allows to compare the results, being the two sets of samples practically equivalent.

During the damaging phases [Figs. 8(a) and 8(c)], the variations of both linear and nonlinear indicators show a nonlinear correlation with the actual load-carrying capacity, in the shape of an exponential decay dependence. The exponential fitting function is reported as a solid line in the plots and the fitting parameters are reported in the legend. Both indicators decrease with increasing actual flexural strength, or conversely increase with increasing damage. The correspondence between the coefficients of the exponential decay for the linear and nonlinear indicators is remarkable, as it can be appreciated in the legend of the corresponding subplots ($k \approx 0.002$).

The correlation during the repairing phases is discussed in Figs. 8(b) and 8(d). Again, an exponential decay law is found, with an offset in both cases due to a noncomplete recovery of the mechanical and ultrasonic properties of the tested specimens. From the mechanical point of view, we notice that only slightly more than 40% of the original ultimate strength is recovered, which is, however, already quite remarkable for practical applications.

The parameters for the exponential decay law (describing the dependence of the linear and nonlinear indicators on the mechanical parameters) are significantly different, as it can be seen from the legend in the corresponding subplots. The value of the exponent for the linear indicator ($k = 0.003$) is comparable with that obtained during the damaging phase, confirming the symmetry between damage progression and damage repair as far as the linear properties are concerned. On the contrary, the coefficient is much larger ($k = 0.009$) for the case of the nonlinear indicator, revealing that the recovery of the nonlinear elastic properties is much faster than the recovery of the linear ones during the repairing phases. As it will be discussed in the next subsection, this asymmetry between damaging and repairing phases suggests the presence of different chemical-physical mechanisms during the repairing process.

In this regard, please note that the correlation laws discussed above should be carefully discussed. The overall behavior, i.e., the nonlinear exponential correlation, could be considered a general rule, even though testing on other samples/geometries should be carried on. On the contrary, the coefficients found for the correlation parameters should not be considered in absolute terms since they depend on the specific geometric setting here adopted. Their reverse analogy with the damaging process could again be a general feature and its assessment and quantification could be crucial when a new repairing system is considered.

B. Evolution of the interface

Starting from the observations and speculations reported in the previous paragraphs, we propose here a possible evolution process of the elastomechanical characteristics of the sample in the cracked zone, that reproduces the observed phenomenology during damage and repair. The description proposed here is based on a very simplified model, with the goal to highlight that very intuitive and simple mechanisms could be proposed to describe qualitatively the observed phenomenology. Thus, without any expectation to explain the physical mechanisms involved in the various processes, the description proposed here is just meant to support the hypotheses/conclusions derived from our measurements about the possible evolution of the interface due to the action of the repairing agent.

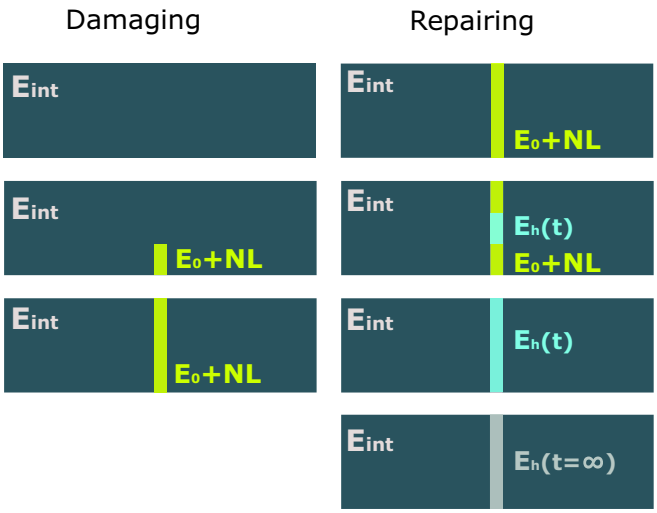

FIG. 9. Schematic representation of the affected zone evolution during damage (left) and repair (right) progression.

1. Phenomenological description

As already remarked, two concurrent phenomena are at play: modulus variation affecting the spectral response and appearance/disappearance of microscopic features resulting in a variation of the nonlinear contributions to signals.

During the damage process, starting from the notch artificially produced in the middle of the sample, a crack is initiated for a given stress-strain state induced by the three-point bending. With progression of the deformation mechanically imposed to the system, the fracture opening and extension increase, generating an affected area surrounding the crack in which several closed microcracks are nucleating and eventually coalesce into an open macrocrack, along the propagation line of the fracture. As a consequence, a thin layer (see the green area in the left column of Fig. 9) is formed with softer effective elastic constant that drastically changes the propagation of elastic waves traveling in the sample. These are mainly reflected at the interface and only partially transmitted due to the high elastic mismatch between the concrete matrix and the air (in the cracked zone). Furthermore, the presence of contact points [2] and/or clapping surfaces [1] at the surfaces of microcracks lead to a local increase of the nonlinear response to an ultrasonic excitation.

During the repairing process, the healing agent in a first stage fills the voids between the two free surfaces (i.e., the open crack area) and, while undergoing a change in viscosity,

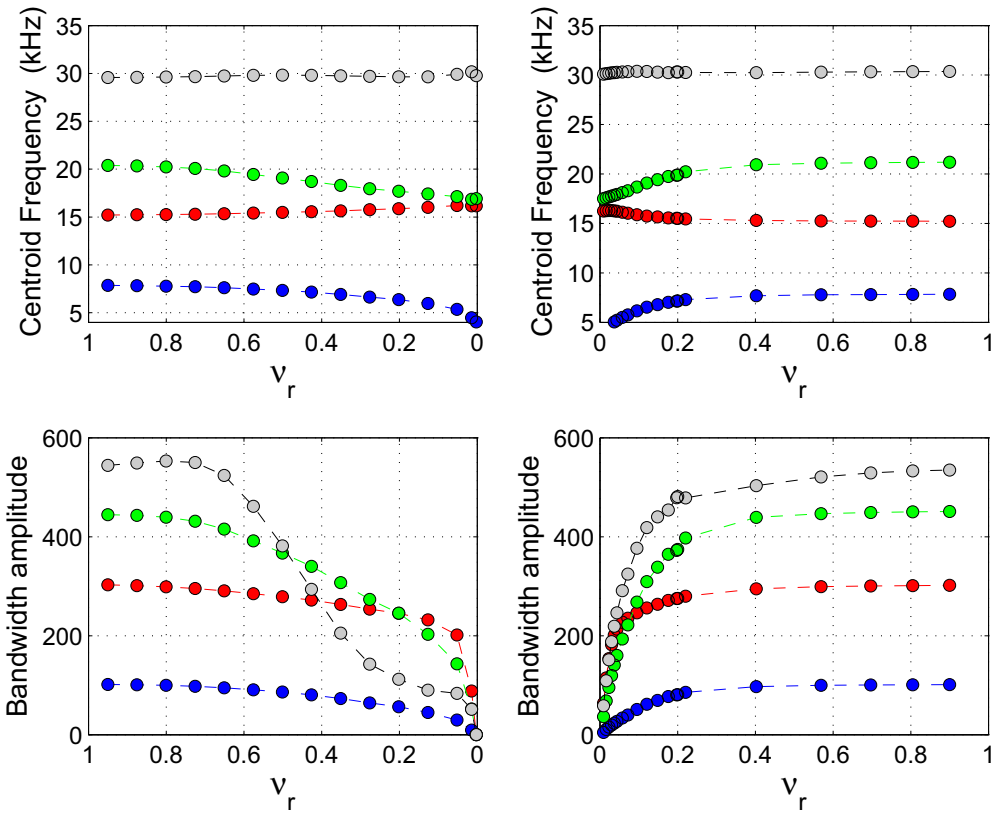

FIG. 10. Simulation results for the centroid frequency and bandwidth amplitude during the damaging (left column) and repairing (right column) phases. Different colors refer to the indicators defined in the four frequency bands. Results should be compared with Fig. 5.

it also fills microcracks, with gradual transition from a liquid to a solid state. During this first stage, the nonlinear response of the sample, that was at its maximum when the sample was completely broken, progressively decreases. The repairing agent, after a short time, starts behaving as an almost solid compound with a softer modulus with respect to that of concrete (see first two subplots in the right column of Fig. 9). Moreover, a progressive complex chemical interaction between the agent and the concrete matrix starts and evolves in time [12,13,38] until the almost complete recovery of the elastic properties in the affected zone. This second phase does not lead to a significant further filling of microcracks, being in this phase the repairing agent already almost solidified.

2. *Model and numerical implementation*

In order to prove the reliability of this schematic description, we performed numerical simulations of the wave propagation in an elastic medium based on a spring model approach [51]. In the model proposed, the specimen (rectangular 2D sample in our simulations, with dimensions 16×4 cm^2) is discretized through a square grid and in each cell the modulus, density, and damping are defined. The cell is then described by a set of springs which, properly arranged, react to a time-dependent stress applied to its surfaces to provide, in the limit of the cell dimension approaching zero, the exact elastodynamic wave propagation equation. The nonlinear part of the stress-strain relation for cells within the crack-affected zone is defined using time-dependent elastic moduli, in which the moduli are calculated at each time as the statistical average of the moduli of linear basic elements which might be in either an elastic or in a rigid state depending on the values of the stress in the cell. This approach, described in details in Refs. [42,44,51], is based on the so-called Preisach-Mayergoytz (PM) description [43]. The multistate PM description adopted is known to be a good model to describe the response of closed cracks and contact points which display different elastic behaviors in compression and tension [39,40] due to deformation effects [41], adhesion phenomena [52,53], dislocations [24], etc. The model was validated in previous works [45,46].

In the simulations, we performed a propagation analysis injecting from the left edge (emitting transducer position) a pulse wave with spectral content at the source similar to the one used in the real experiments. On the right side of the sample (receiver position) we recorded the elastic response. We first assumed to have no crack-affected zone and fixed the linear elastic parameters (Lamé constants $\lambda = 5$ GPa, $\mu = 11$ GPa, i.e., Young's modulus $E = \lambda + 2\mu = 27$ GPa, $\rho = 2800$ kg/m^3) to obtain a spectral response similar to that experimentally observed. Then, the simulation was repeated several times, each time changing the extension of the affected zone: a thin layer (0.5 mm thick) with increasing/decreasing length (see Fig. 9). In particular, note the following

(i) damaging: the affected zone was increased in extent and the corresponding discretization cells were assigned a very soft modulus ($E_0 = 100$ kPa, $\rho = 1.2$ Kg/m^3) and nonlinear properties;

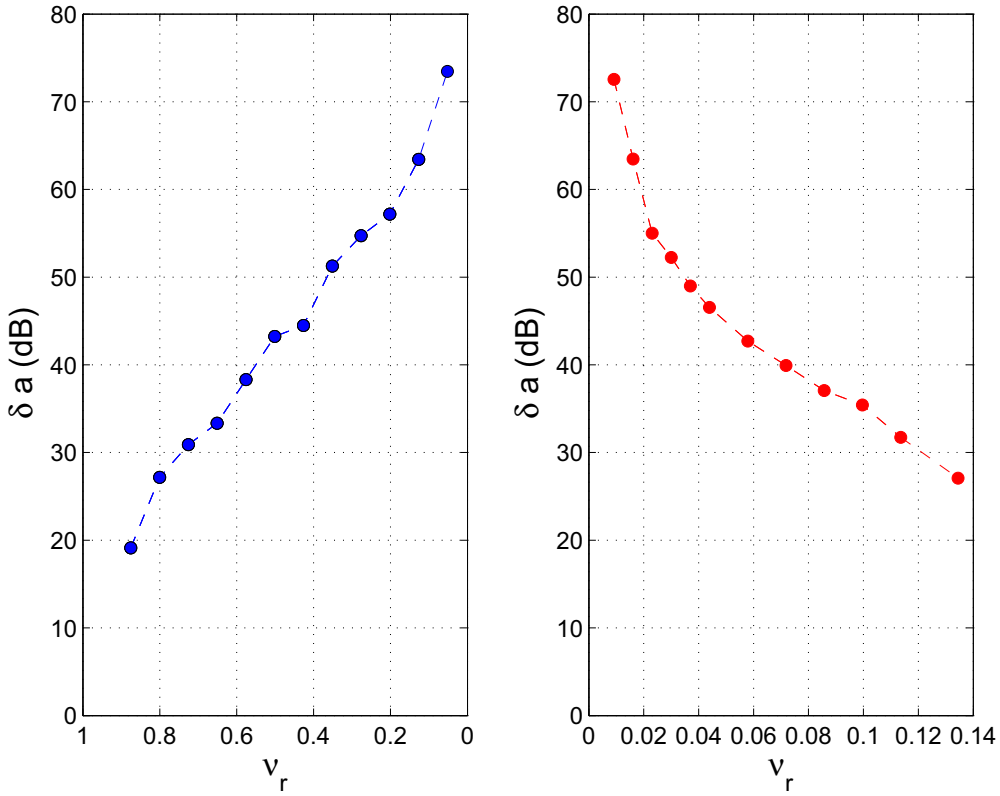

FIG. 11. Simulation results obtained by the nonlinear SSM analysis during damage (left plot) and repair (right plot). Results should be compared with Fig. 6.

(ii) repairing, phase 1: cells within the affected zone were progressively replaced by cells with a soft modulus [$E_h(t)$ in Fig. 9] and linear behavior;

(iii) repairing, phase 2: cells within the affected zone were further replaced by cells with an elastic modulus evolving to the original elastic value [$\lim_{t\to\infty} E_h(t) = E_{\text{int}}$].

Note that, during repairing, phases 1 and 2 are overlapped.

In order to characterize the damage-affected zone for each of the simulations performed, we defined a damage indicator ν_r that measures the ratio between the actual mean longitudinal wave velocity in the affected zone and the longitudinal velocity in the intact sample:

$$\nu_r = \frac{\int v_L dl}{v_{\text{int}} L}, \tag{8}$$

where v_L ($v_L = \sqrt{E/\rho}$) is the longitudinal wave velocity of the dl element of the layer, v_{int} is the longitudinal wave velocity of the intact sample, and L is the length of the vertical section of the sample. The parameter ν_r is the simulation counterpart of the quantities D and "healing time" (see Fig. 5).

3. Numerical results

Simulations were performed for different configurations of the damage-affected zone, repeating the very same analysis as for the experimental data, in order to estimate the centroid frequency, bandwidth amplitude, and the nonlinear parameter a. They are plotted as a function of ν_r [see Eq. (8)] in Figs. 10 and 11. In the simulations of the damaging process we reproduced only the cases corresponding to positive D values, i.e., to the crack opening and propagation stages.

Numerical results for the linear indicators during damaging and repairing are shown in Fig. 10. The qualitative agreement between the numerical and the experimental results (Fig. 5) is good. Indeed, simulations during damaging (repairing) predict the smooth decreasing (increasing) in the centroid frequency of the first and third bands and, correspondingly, a drop down (rise up) of all the bandwidth amplitudes. Moreover, a different time scale is observed in the recovery of the bandwidth amplitude for the different modes: as in the experiments, the second mode amplitude (red color in the figure) almost regains the original value well before the other modes. This happens at $\nu_r \approx 0.2$, i.e., in correspondence of the beginning of the second phase of repairing (i.e., after substantial solidification of the healing agent) which means that the attenuation of this mode is mainly due to nonlinear attenuation effects.

We also performed the analysis of the nonlinear behavior, as shown in Fig. 11: here, on the left (right) the nonlinear parameter is evaluated in the damaging (repairing) phases as a function of ν_r [see Eq. (8)]. Again, the agreement with the experimental observations is good and in particular the faster time scale for a to recover the original intact value is evident during the repairing phase.

V. CONCLUSIONS

In this paper, we analyzed the evolution of the elastic and mechanical properties of concrete samples as a function of the progression of a damage process (caused by cycles of

flexural solicitations), followed by a repair process (induced by a sodium silicate layer acting as a repairing agent for the damaged specimen). Linear/nonlinear ultrasonic tests and mechanical flexural tests were used for the experimental observations. The existence of a correlation between elastic and mechanical properties was demonstrated. Also, the symmetry between damaging and repairing processes was analyzed and discussed.

The time scales observed during the repair process, respectively, for the recovery of the linear and of the nonlinear elastic properties turned out to be different. Based on this observation, a possible explanation was proposed for the evolution of the physical properties around the damaged zone. While the damaging phases correspond to a progressive crack opening, with consequent variation of the effective local modulus (softening) and generation of contact tips responsible for the increase of nonlinearity, the situation is more complex during the repairing phases. Here, aside from crack closing due to the penetration, gelation, and solidification of the repairing agent, chemical reactions with the concrete matrix occur on a longer time scale, leading to a full recovery which, in the case of sodium silicate, took place in about 4 weeks. Model results are in good agreement with the experimental observations. Further verification of the proposed description for the link between microstructural evolution and damage/repair progression is ongoing, with reference to a system in which a different repairing agent is used instead of sodium silicate, preventing the occurrence of chemical reactions with the cement matrix [54].

ACKNOWLEDGMENTS

The authors thank Fondazione CRT for funding this study in the framework of the research project "SHEcrete: Development of advanced Self-HEaling concrete systems with improved reliability and durability." The contribution of COST Action No. CA15202 "SARCOS: Self-healing As preventive Repair of COncrete Structures" is also gratefully acknowledged.

[1] V. Tournat, V. Zaitsev, V. Gusev, V. Nazarov, P. Béquin, and B. Castagnède, Probing Weak Forces in Granular Media Through Nonlinear Dynamic Dilatancy: Clapping Contacts and Polarization Anisotropy, Phys. Rev. Lett. **92**, 085502 (2004).

[2] V. Aleshin and K. Van Den Abeele, Microcontact-based theory for acoustics in microdamaged materials, J. Mech. Phys. Solids **55**, 366 (2007)

[3] K. H. Matlack, J. J. Wall, J.-Y. Kim *et al.*, Evaluation of radiation damage using nonlinear ultrasound, J. Appl. Phys. **111**, 054911 (2012).

[4] K. Van Tittelboom and N. De Belie, Self-healing in cementitious materials: A review, Materials **6**, 2182 (2013).

[5] A. Formia, S. Terranova, P. Antonaci, N. Pugno, and J. M. Tulliani, Setup of extruded cementitious hollow tubes as containing/releasing devices in self-healing systems, Materials **8**, 1897 (2015).

[6] B. Hillouin, K. Van Tittelboom, E. Gruyaert, N. De Belie, and A. Loukili, Design of polymeric capsules for self-healing concrete, Cem. Concr. Compos. **55**, 298 (2015).

[7] A. Kwiecien, M. Gruszczynski, and B. Zajac, Tests of flexible polymer joints repairing of concrete pavements and of polymer modified concretes influenced by high deformations, Key Eng. Mater. **466**, 225 (2011).

[8] M. Sanchez, M. C. Alonso, and R. Gonzales, Preliminary attempt of hardened mortar sealing by colloidal nanosilica migration, Costr. Build. Mater. **66**, 306 (2014).

[9] V. Zaitsev, P. Richard, R. Delannay, V. Tournat, and V. Gusev, Pre-avalanche structural rearrangements in the bulk of granular medium: Experimental evidence, Europhys. Lett. **83**, 64003 (2008).

[10] S. Kiesgen de Richter, V. Zaitsev, P. Richard, R. Delannay, G. Le Caër, and V. Tournat, Experimental evidence of ageing and slow restoration of the weak-contact configuration in tilted 3D granular packings, J. Stat. Mech. (2010) P11023.

[11] V. Zaitsev, V. Gusev, V. Tournat, and P. Richard, Slow Relaxation and Aging Phenomena at the Nanoscale in Granular Materials, Phys. Rev. Lett. **112**, 108302 (2014).

[12] M. Ait Ouarabi, P. Antonaci, F. Boubenider, A. S. Gliozzi, and M. Scalerandi, Ultrasonic monitoring of the interaction between cement matrix and alkaline silicate solution in self-healing systems, Materials **10**, 46 (2017).

[13] P. Alghamri, A. Kannellopoulos, and A. Al-Tabbaa, Impregnation and encapsulation of lightweight aggregates for self-healing concrete, Constr. Build. Mater. **124**, 910 (2016).

[14] A. J. Crosby, K. R. Shull, H. Lakrout *et al.*, Deformation and failure modes of adhesively bonded elastic layers, J. Appl. Phys. **88**, 2956 (2000).

[15] F. Moradi-Marani, P. Rivard, C. P. Lamarche *et al.*, Evaluating the damage in reinforced concrete slabs under bending test with the energy of ultrasonic waves, Constr. Build. Mater. **73**, 663 (2014).

[16] M. A. Adam, M. Said, A. A. Mahmoud, and A. S. Shanour, Analytical and experimental flexural behavior of concrete beams reinforced with glass fiber reinforced polymer bars, Constr. Build. Mater. **84**, 354 (2015).

[17] F. G. Mitri and M. Fatemi, Improved vibroacoustography imaging for nondestructive inspection of materials, J. Appl. Phys. **98**, 114901 (2005).

[18] I. Solodov, J. Bai, and G. Busse, Resonant ultrasound spectroscopy of defects: Case study of flat-bottomed holes, J. Appl. Phys. **113**, 223512 (2013).

[19] A. A. Shah and Y. Ribakov, Non-destructive evaluation of concrete in damaged and undamaged states, Mater. Design **30**, 3504 (2009).

[20] M. Scalerandi, S. Idjimarene, M. Bentahar, and R. El Guerjouma, Evidence of evolution of microstructure in solid elastic media based on a power law analysis, Commun. Nonlin. Sci. Numer. Simul. **22**, 334 (2015).

[21] M. Bentahar, H. El Aqra, R. El Guerjouma, M. Griffa, and M. Scalerandi, Hysteretic elasticity in damaged concrete: Quantitative analysis of slow and fast dynamics, Phys. Rev. B **73**, 014116 (2006).

[22] C. Payan *et al.*, Applying nonlinear resonant ultrasound spectroscopy to improving thermal damage assessment in concrete, J. Acoust. Soc. Am. **121**, EL125 (2007).

[23] L. Quan, X. Z. Liu, and X. F. Gong, Nonlinear nonclassical acoustic method for detecting the location of cracks, J. Appl. Phys. **112**, 054906 (2012).

[24] C. Mechri, M. Scalerandi, and M. Bentahar, Enhancement of harmonics generation in hysteretic elastic media induced by conditioning, Commun. Nonlin. Sci. Numer. Simul. **45**, 117 (2017).

[25] M. Scalerandi, A. S. Gliozzi, C. L. E. Bruno, D. Masera, and P. Bocca, A scaling method to enhance detection of a nonlinear elastic response, Appl. Phys. Lett. **92**, 101912 (2008).

[26] M. Scalerandi, A. S. Gliozzi, C. L. E. Bruno, and P. Antonaci, Nonequilibrium and hysteresis in solids: Disentangling conditioning from nonlinear elasticity, Phys. Rev. B **81**, 104114 (2010).

[27] M. Ait Ouarabi, F. Boubenider, A. S. Gliozzi, and M. Scalerandi, Nonlinear coda wave analysis of hysteretic elastic behavior in strongly scattering elastic media, Phys. Rev. B **94**, 134103 (2016).

[28] P. Antonaci, A. Formia, A. S. Gliozzi, M. Scalerandi, and J. M. Tulliani, Diagnostic application of nonlinear ultrasonics to characterize degradation by expansive salts in masonry systems, NDT E Int. **55**, 57 (2013).

[29] D. M. Joglekar and M. Mitra, Time domain analysis of nonlinear frequency mixing in a slender beam for localizing a breathing crack, Smart Mater. Struct. **26**, 025009 (2016).

[30] I. Solodov, J. Wackerl, K. Pfleiderer, and G. Busse, Nonlinear self-modulation and subharmonic acoustic spectroscopy for damage detection and location, Appl. Phys. Lett. **84**, 5386 (2004).

[31] K. Van den Abeele and J. De Visscher, Damage assessment in reinforced concrete using spectral and temporal nonlinear vibration techniques, Cem. Concr. Res. **30**, 1453 (2000).

[32] M. Scalerandi, M. Griffa, P. Antonaci, M. Wyrzykowski, and P. Lura, Nonlinear elastic response of thermally damaged consolidated granular media, J. Appl. Phys. **113**, 154902 (2013).

[33] J. Wang, K. Van Tittelboom, N. De Belie, and W. Verstraete, Use of silica gel or polyurethane immobilized bacteria for self-healing concrete, Constr. Build. Mater. **26**, 532 (2012).

[34] K. Van Tittelboom, N. De Belie, F. Lehmann, and C. U. Grosse, Acoustic emission analysis for the quantification of autonomous crack healing in concrete, Constr. Build. Mater. **28**, 333 (2012).

[35] B. Hillouin, D. Hillouin, F. Grondin *et al.*, Mechanical regains due to self-healing in cementitious materials: Experimental measurements and micro-mechanical model, Cem. Concr. Res. **80**, 21 (2016).

[36] A. Formia, S. Irico, F. Bertola, F. Canonico, P. Antonaci, N. Pugno, and J. M. Tulliani, Experimental analysis of self-healing cement-based materials incorporating extruded cementitious hollow tubes, J. Intell. Mater. Syst. Struct. **27**, 2633 (2016).

[37] Standard UNI EN 196-1 Methods of testing cement, Part 1: Determination of strength.

[38] S. S. Kouassi, M. T. Tognonvi, J. Soro, and S. Rossignol, Consolidation mechanism of materials obtained from sodium silicate solution and silica-based aggregates, J. Non-Cryst. Solids **357**, 3013 (2011).

[39] R. A. Guyer and P. A. Johnson, Nonlinear mesoscopic elasticity: Evidence for a new class of materials, Phys. Today **52**(4), 30 (1999).

[40] A. G. Zhou, S. Basu, G. Friedman, P. Finkel, O. Yeheskel, and M. W. Barsoum, Hysteresis in kinking nonlinear elastic solids and the Preisach-Mayergoyz model, Phys. Rev. B **82**, 094105 (2010).

[41] S. Delrue and K. Van den Abeele, Three-dimensional finite element simulation of closed delaminations in composite materials, Ultrasonics **52**, 315 (2012).

[42] M. Scalerandi, A. S. Gliozzi, and S. Idjimarene, Power laws behavior in multi-state elastic models with different constraints in the statistical distribution of elements, Commun. Nonlin. Sci. Numer. Simul. **19**, 3628 (2014).

[43] R. A. Guyer, K. R. McCall, and G. N. Boitnott, Quantitative implementation of Preisach-Mayergoyz space to find static and dynamic elastic moduli in rock, J. Geophys. Res. **102**, 5281 (1997).

[44] M. Nobili and M. Scalerandi, Temperature effects on the elastic properties of hysteretic elastic media: Modeling and simulations, Phys. Rev. B **69**, 104105 (2004).

[45] M. Scalerandi, P. P. Delsanto, P. A. Johnson *et al.*, Stress induced conditioning and thermal relaxation in the simulation of quasi-static compression experiments, J. Phys. D: Appl. Phys. **36**, 288 (2003).

[46] A. S. Gliozzi, M. Griffa, and M. Scalerandi, Efficiency of time-reversed acoustics for nonlinear damage detection in solids, J. Acoust. Soc. Am. **120**, 2506 (2006).

[47] M. Bentahar, R. El Guerjouma, S. Idijmarene, and M. Scalerandi, Influence of noise on the threshold for detection of elastic nonlinearity, J. Appl. Phys. **113**, 043516 (2013).

[48] V. Zaitsev and L. Matveev, Strain-amplitude dependent dissipation in linearly dissipative and nonlinear elastic microinhomogeneous media, Russ. Geol. Geophys. **47**, 694 (2006).

[49] C. Payan, T. J. Ulrich, P. Y. Le Bas, T. Saleh, and M. Guimaraes, Quantitative linear and nonlinear resonance inspection techniques and analysis for material characterization: Application to concrete thermal damage, J. Acoust. Soc. Am. **136**, 537 (2014).

[50] G. Renaud *et al.*, Anisotropy of dynamic acoustoelasticity in limestone, influence of conditioning, and comparison with nonlinear resonance spectroscopy, J. Acoust. Soc. Am. **133**, 3706 (2013).

[51] P. P. Delsanto and M. Scalerandi, Modeling nonclassical nonlinearity, conditioning, and slow dynamics effects in mesoscopic elastic materials, Phys. Rev. B **68**, 064107 (2003).

[52] V. Gusev and N. Chigarev, Nonlinear frequency-mixing photoacoustic imaging of a crack: Theory, J. Appl. Phys. **107**, 124905 (2010).

[53] C. Pecorari, Adhesion and nonlinear scattering by rough surfaces in contact: Beyond the phenomenology of the Preisach-Mayergoyz framework, J. Acoust. Soc. Am. **116**, 1938 (2004).

[54] P. Antonaci, G. Anglani, A. S. Gliozzi, M. Scalerandi, and L. Salini, Comparative ultrasonic investigation on the behaviour of different repairing agents for self-healing concrete applications (unpublished).